

RSC Advances



This is an *Accepted Manuscript*, which has been through the Royal Society of Chemistry peer review process and has been accepted for publication.

Accepted Manuscripts are published online shortly after acceptance, before technical editing, formatting and proof reading. Using this free service, authors can make their results available to the community, in citable form, before we publish the edited article. This *Accepted Manuscript* will be replaced by the edited, formatted and paginated article as soon as this is available.

You can find more information about *Accepted Manuscripts* in the [Information for Authors](#).

Please note that technical editing may introduce minor changes to the text and/or graphics, which may alter content. The journal's standard [Terms & Conditions](#) and the [Ethical guidelines](#) still apply. In no event shall the Royal Society of Chemistry be held responsible for any errors or omissions in this *Accepted Manuscript* or any consequences arising from the use of any information it contains.

Host matrix impact on Er³⁺ upconversion emission and its temperature dependence

A.K. Singh,^{1*} Praveen Kumar Shahi,² S. B. Rai², Bruno Ullrich^{1,3}

¹Instituto de Ciencias Físicas, Universidad Nacional Autónoma de México, Cuernavaca, Morelos 62210, Mexico

²Department of Physics, Banaras Hindu University, Varanasi-221005, India

³Ullrich Photonics LLC, Wayne Ohio 43466, USA

Abstract

By synthesizing $Y_{(1.9-2x)}Yb_{0.1}Er_{2x}O_3$, $Y_{(0.95-x)}Yb_{0.05}Er_xVO_4$ and $Y_{(0.95-x)}Yb_{0.05}Er_xPO_4$ phosphors, with phonon frequency maxima at 560, 826 and 1050 cm^{-1} , respectively, we present the impact of phonon energy and crystal structure of the host matrix on upconversion and temperature sensing behavior. The spectral upconversion characteristics of all three phosphors reveal noticeably differences. The temperature sensing studies reveal that the phosphors have maximum sensitivity $\sim 490K$, which is found to be highest ($0.0105K^{-1}$) in $Y_{0.947}Yb_{0.05}Er_{0.003}VO_4$ followed by $Y_{1.894}Yb_{0.1}Er_{0.006}O_3$ and $Y_{0.947}Yb_{0.05}Er_{0.003}PO_4$ phosphors. We found that the temperature sensitivity basically depends on intensity ratio of two thermally coupled emission bands, ${}^2H_{11/2} \rightarrow {}^4I_{15/2}$ and ${}^4S_{3/2} \rightarrow {}^4I_{15/2}$, of Er^{3+} . Further, the intensity ratio depends on phonon energy of the host lattice, crystal structure, surface quenching centers and the temperature dependence of non-radiative decay rate.

Keywords: Optical properties, lanthanide, luminescence, upconversion, temperature sensor

Corresponding author: akhilesh_singh343@yahoo.com

1. Introduction

Conventional methods of temperature measurements, which employ, for example liquid-filled thermometers, thermocouples, and thermistors are not applicable for temperature measurement of objects below 10 μm size.¹ Consequently, temperature sensing in the microcosm requires altered, non-traditional probing techniques. This can be done with luminescence-based temperature sensors, which can be used for biological and technological applications, such as measuring the temperature of microfluids and microcircuits, to name a few.²⁻³ The here pursued principle basically uses lanthanide ions as a luminescence center, whilst the emission intensity, lifetime or intensity ratio of two-thermally coupled bands is monitored as a function of temperature to record the temperature of an object.⁴⁻¹⁰

Luminescence intensity and lifetime-based temperature sensing is generally performed in lanthanide complexes or lanthanide-based inorganic-organic hetero-paired nanostructures. However, the use of ultraviolet light as an excitation source limits their biological applicability,¹¹⁻¹² and additionally, power fluctuations and other environmental effects might influence the performance. On the other hand, temperature probing by means of luminescence intensity ratio variations overcomes these problems. The lanthanide which is commonly used for this purpose are Er^{3+} , Ho^{3+} , Tm^{3+} , *etc.* The advantage with these ions is that they show efficient upconversion (UC) under near infrared (NIR) irradiation exposure, and therefore, are suitable for biological applications as well. It is important to note that temperature measurements relying on luminescence intensity ratios contain the precise information about the temperature in a single emission spectrum and are not influenced by intensity variations of the excitation source and photo detector drifts. In literature mainly Er^{3+} , Ho^{3+} , Nd^{3+} and Tm^{3+} doped phosphors have been used for temperature sensing.⁸⁻¹⁰ Among them Er^{3+} activated phosphors are preferred because of

strong UC emission intensities for the thermally-coupled levels ($^2H_{11/2}$ and $^4S_{3/2}$). The nature of temperature versus sensitivity plots reported in literature varies in different phosphors.¹⁻¹⁰ Bearing in mind that the host lattice phonon energy affects the UC emission, it may also alter the sensitivity of temperature sensor.¹³⁻¹⁶ Therefore, it is important to investigate the role of host matrix (phonon energy, crystal structure, *etc.*) on UC emission and temperature sensing characteristics. In order to perform this study, which - to the best of our knowledge - cannot be found in the literature, we have synthesized $Y_{(1.9-2x)}Yb_{0.1}Er_{2x}O_3$, $Y_{(0.95-x)}Yb_{0.05}Er_xVO_4$ and $Y_{(0.95-x)}Yb_{0.05}Er_xPO_4$ phosphors by a solid state reaction method and studied the UC emission and its potential for temperature sensing.

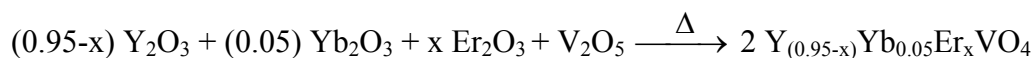
2. Experimental

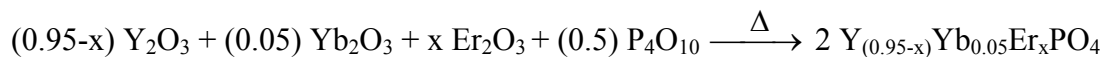
2.1 Materials

Analytical reagent (AR) grade yttrium oxide (Y_2O_3 , 99.99%, Himedia), vanadium pentoxide (V_2O_5 , 99.9%, Loba Chemicals), phosphorus pentoxide (P_4O_{10} (empirical formula P_2O_5), 99.9%, Loba Chemicals), ytterbium oxide (Yb_2O_3 , 99.9%, Aldrich) and erbium oxide (Er_2O_3 , 99.9%, Aldrich) were used for the synthesis of $Y_{(1.9-2x)}Yb_{0.1}Er_{2x}O_3$, $Y_{(0.95-x)}Yb_{0.05}Er_xVO_4$ and $Y_{(0.95-x)}Yb_{0.05}Er_xPO_4$ phosphors.

2.2 Synthesis

For the synthesis of $Y_{(1.9-2x)}Yb_{0.1}Er_{2x}O_3$, $Y_{(0.95-x)}Yb_{0.05}Er_xVO_4$ and $Y_{(0.95-x)}Yb_{0.05}Er_xPO_4$ ($x=0.003$, 0.01, and 0.02) phosphors the following, stoichiometric amounts of raw materials were mixed homogeneously in an agate mortar using AR grade acetone as a mixing medium:





Afterwards, the samples were kept at ambient temperature for overnight drying. The mixture was then placed in an alumina crucible and calcined in high temperature furnace at the optimized temperature of 1523K for 5h. For the temperature sensing experiments, phosphor samples were produced in pellet form with diameter and thickness of 12 and 1.5 mm, respectively, and were sintered at 1573 K for 5 h.

2.3 Characterization

X-ray diffraction (XRD) patterns and Fourier transform infrared (FTIR) transmission spectra (from 400 to 4000 cm^{-1} with a resolution of 2 cm^{-1}) of the samples were measured with a Rigaku (MiniFlex II DEXTOP) powder diffractometer ($\text{CuK}\alpha$ radiation (1.5404 Å)) and a Thermo Scientific FTIR spectrometer (NICOLET 6700), respectively. The down-shifting (DS) PL measurements were performed employing the fluorolog-3 spectrofluorometer (FL3-11, Horiba Jobin Yvon) equipped with a 450 W xenon flash lamp. The DS lifetime measurements were carried out with a pulsed xenon lamp (25 W) by the same setup. The UC luminescence was excited by the 976 nm emission of a tunable continuous wave (cw) 2 W diode laser, while the data collection was addressed via the conjunction of aiHR 320 (Horiba JobinYvon) spectrometer with an attached R928P photomultiplier tube (PMT). For the lifetime measurement of the $^2\text{H}_{11/2}$ and $^4\text{S}_{3/2}$ levels the laser beam was mechanically chopped at 10 Hz and the data were acquired using analog digital scope-HM1507 running software SP107. To measure the UC emission at different temperatures, the pellets were mounted on a homemade heating device, whereas the laser was focused near to the pellet edge keeping the thermocouple in close proximity (within ~4 mm) to the focal spot.

3. Results and discussion

3.1 Structural analysis

In order to check the phase purity and to determine the crystal structure parameters, Rietveld analyses of the powder diffraction data have been carried out using the crystal structure refinement program “FULLPROF”.¹⁷ The Pseudo-Voigt function has been used to define the peak profile. In case of the $Y_{1.894}Yb_{0.1}Er_{0.006}O_3$ phosphor all the diffraction peaks match well using $Ia-3$ (206) space group (JCPDS no. 41-1105) of cubic structure. The structure provides two cation symmetry sites, C_2 and C_{3i} , with six-fold oxygen coordination. The Wyckoff positions for these two cationic sites are 8b and 24d with local symmetry C_{3i} and C_2 , respectively, whilst oxygen ions are located at 48e Wyckoff positions. The $Y_{0.947}Yb_{0.05}Er_{0.003}VO_4$ and $Y_{0.947}Yb_{0.05}Er_{0.003}PO_4$ phosphors have zircon type tetragonal crystal structure with space group $I41/amd$ (141). The Wyckoff positions for Y, V(P) and O are 4a, 4b and 16h, respectively. In this structure, Y and V(P) are surrounded by eight oxygen atoms having two different bond lengths and by four oxygen atoms with equal bond lengths, respectively, and between YO_8 and VO_4 (PO_4) units two oxygen atoms are corner-sharing. The VO_4 (PO_4) (tetrahedron) has S_4 symmetry, whilst YO_8 (dodecahedron) has D_{2d} symmetry. The Yb/Er atoms substitute Y sites in the lattice. Figure 1 depicts the Rietveld fits for $Y_{1.894}Yb_{0.1}Er_{0.006}O_3$, $Y_{0.947}Yb_{0.05}Er_{0.003}VO_4$ and $Y_{0.947}Yb_{0.05}Er_{0.003}PO_4$ phosphors, indicating a good agreement between observed and calculated XRD patterns. The refinement parameters are given in table 1. The XRD analysis clearly depicts that $Y_{1.894}Yb_{0.1}Er_{0.006}O_3$ and $Y_{0.947}Yb_{0.05}Er_{0.003}VO_4$ are phase pure, whereas $Y_{0.947}Yb_{0.05}Er_{0.003}PO_4$ has small surplus of unreacted Y_2O_3 .

To determine the phonon frequency of the host lattices, we monitored the FTIR spectra of $Y_{1.894}Yb_{0.1}Er_{0.006}O_3$, $Y_{0.947}Yb_{0.05}Er_{0.003}VO_4$ and $Y_{0.947}Yb_{0.05}Er_{0.003}PO_4$ phosphors (see Fig. 2). The

$Y_{1.894}Yb_{0.1}Er_{0.006}O_3$ shows a strong sharp peak due to the stretch of the Y-O bond at 560 cm^{-1} , and $Y_{0.947}Yb_{0.05}Er_{0.003}VO_4$ and $Y_{0.947}Yb_{0.05}Er_{0.003}PO_4$ show intense peaks due to stretches of the V-O and P-O bonds at 826 and 1050 cm^{-1} , respectively.^{14, 18} In $Y_{0.947}Yb_{0.05}Er_{0.003}PO_4$ phosphor, the FTIR peaks at 523 and 638 cm^{-1} correspond to bending vibrations of P-O bonds.¹⁹ Thus, the FTIR studies reveal that all these host matrices possess considerably different phonon frequencies.

3.2 Upconversion

The UC emission spectra of $Y_{0.947}Yb_{0.05}Er_{0.003}PO_4$, $Y_{0.947}Yb_{0.05}Er_{0.003}VO_4$ and $Y_{1.894}Yb_{0.1}Er_{0.006}O_3$ are shown in Fig. 3. The $Y_{1.894}Yb_{0.1}Er_{0.006}O_3$ and $Y_{0.947}Yb_{0.05}Er_{0.003}VO_4$ phosphors show blue emission bands around 410 nm because of three-photon processes.⁸ The blue emission is more intense in $Y_{1.894}Yb_{0.1}Er_{0.006}O_3$ than in $Y_{0.947}Yb_{0.05}Er_{0.003}VO_4$ phosphor, most likely owing to the higher phonon energy of YVO_4 host. The equivalent argument explains the absence of blue emission of $Y_{0.947}Yb_{0.05}Er_{0.003}PO_4$. The emission bands observed at 380 , 410 , 488 , 523 , 548 and 660 nm correspond to the ${}^4G_{11/2} \rightarrow {}^4I_{15/2}$, ${}^2H_{9/2} \rightarrow {}^4I_{15/2}$, ${}^2H_{9/2} \rightarrow {}^4I_{15/2}$, ${}^4F_{7/2} \rightarrow {}^4I_{15/2}$, ${}^2H_{11/2} \rightarrow {}^4I_{15/2}$, ${}^4S_{3/2} \rightarrow {}^4I_{15/2}$ and ${}^4F_{9/2} \rightarrow {}^4I_{15/2}$ transitions of Er^{3+} ion, respectively.⁵⁻⁸ It can also be noticed that all the emission bands show Stark components. The energy level splitting is the largest in $Y_{1.894}Yb_{0.1}Er_{0.006}O_3$ because of the difference in crystal field potential/distance between Er^{3+} and O^{2-} (ligands) due to different crystal structure of the phosphors.²⁰⁻²¹

In order to explain the origin of the UC emission transitions of the phosphors, Fig. 4 displays the energy level diagram of the Er^{3+} and Yb^{3+} ions. Basically, there are two distinct processes, i.e., the excited state absorption (ESA) and energy transfer (ET), which are responsible for the UC emission. The Er^{3+} ion in its ground state absorbs the incident NIR photon (ground state absorption, GSA) resulting in the resonant excitation of the ${}^4I_{11/2}$ level, from

where, via the absorption of a second photon the ${}^4F_{7/2}$ level gets excited. As a result, the excitation scheme refers to a non-coherent two photon process. Instead re-excitation (from ${}^4I_{11/2}$ level), however, the ion can relax to ${}^4I_{13/2}$ level from where it can absorb a second photon and populate ${}^4F_{9/2}$ level. The ion in ${}^4F_{9/2}$ level can absorb a third photon populating the ${}^2H_{9/2}$ level, or relaxes into the ${}^4I_{15/2}$ level by emitting light at 660 nm. The ion in the ${}^4F_{7/2}$ level can emit at 488 nm by relaxing to level ${}^4I_{15/2}$, or through multiphonon non-radiative relaxation can populate the ${}^2H_{11/2}$ and ${}^4S_{3/2}$ levels. There are three possibilities for depopulation from these two levels: (i) Emission at 523 and 548 nm via the ${}^2H_{11/2} \rightarrow {}^4I_{15/2}$ and ${}^4S_{3/2} \rightarrow {}^4I_{15/2}$ transitions, respectively, (ii) further relaxation to the ${}^4F_{9/2}$ level, or (iii) the ion gets re-excited in the ${}^4G_{7/2}$ level by the absorption of a third photon. The latter transition may result in blue and ultraviolet (UV) emissions.

It is important to stress at this point that the Er^{3+} ion itself has a very weak emission due to the low absorption cross section ($1.7 \times 10^{-21} \text{ cm}^2$). However, by considering the factor 7 times greater absorption cross section ($11.7 \times 10^{-21} \text{ cm}^2$) of the Yb^{3+} ion, the emission of the Yb^{3+}/Er^{3+} co-doped samples can be increased by the energy transfer from Yb^{3+} to Er^{3+} ion.⁵ Additionally, keeping a concentration ratio of $Yb^{3+}/Er^{3+} = 16.7$, the possibility of photon absorption by Yb^{3+} is considerably gained in comparison to Er^{3+} . Figure 4 shows that the Yb^{3+} can transfer single photon energy through different ways or it can transfer energy of two photons simultaneously through cooperative energy transfer (CET) process to ${}^4F_{7/2}$ level of Er^{3+} ion. The UC emission in Yb^{3+}/Er^{3+} co-doped phosphors for the given concentrations is basically due to ET process, while the probability of ESA and CET processes are very low.²²

It is clearly of importance to discuss the reasons for the different green/red (G/R) emission intensity ratios in Fig. 3, which are ~ 46.88 , ~ 2.66 , and ~ 5.18 (calculated by taking the

ratio of integrated UC emission intensity of 500-586 nm and 625-720 nm regions) for $Y_{0.947}Yb_{0.05}Er_{0.003}VO_4$, $Y_{0.947}Yb_{0.05}Er_{0.003}PO_4$, and $Y_{1.894}Yb_{0.1}Er_{0.006}O_3$, respectively. To study the scatter of G/R intensity ratios, we prepared phosphors with different concentrations and recorded their DS and UC emission spectra, which are shown in Fig. 5 for $Y_{1.86}Yb_{0.1}Er_{0.04}O_3$, $Y_{0.93}Yb_{0.05}Er_{0.02}VO_4$, and $Y_{0.93}Yb_{0.05}Er_{0.02}PO_4$ phosphors (spectra for $x=0.02$ composition are shown, because of higher possibility of red emission). The DS emission spectra of phosphors do not show red emission band, whereas it is observed in the UC emission spectra. Figure S1 reveals that the intensity of the red emission band changes very little with Er^{3+} ion concentration ($x=0.003$ to 0.02), but it significantly affected the G/R intensity ratio in $Y_{(0.95-x)}Yb_{0.05}Er_xVO_4$ phosphors. The UC emission spectrum of $Y_{1.994}Er_{0.006}O_3$ phosphor, shown in Figure S2, reveals only green emission bands, but an addition of Yb^{3+} ion in this phosphor ($Y_{1.894}Yb_{0.1}Er_{0.006}O_3$) causes the prominent red emission band. This observation suggests that - along with the overall UC emission change - the Yb^{3+} ion is also responsible for the G/R intensity alterations. The absence of the red emission band in the DS spectra clearly shows that mainly the ET process is the origin of the red emission band in UC spectrum, i.e. ion in the $^4I_{13/2}$ level receives the energy via non-resonant energy transfer (most likely from Yb^{3+}) and populates $^4F_{9/2}$ level from where relaxation to the $^4I_{15/2}$ level occurs - during the emission of red light emission at 660 nm.²²⁻²⁵ Thus, the difference in the G/R intensity ratio is basically due to the difference in lifetime of $^4I_{11/2}$ and $^4I_{13/2}$ levels in different host matrices. The lifetime of Er^{3+} levels in YVO_4 host is significantly different than in other host matrices. Figure S3 reveals that the lifetime of the $^4S_{3/2}$ level of Er^{3+} ion in YVO_4 is an order of magnitude less than in Y_2O_3 and YPO_4 host matrices. The shorter lifetime of the $^4S_{3/2}$ level of Er^{3+} in YVO_4 could be attributed to wavefunction coupling between 3d orbital of V^{5+} and 4f orbital of Er^{3+} . In YVO_4 the energy levels of $^2H_{11/2}$

and $^4S_{3/2}$ of Er^{3+} are close to the $3T_1$ level of the V 3d orbital. These adjacent positions provoke strong coupling between the $^2H_{11/2}$, $^4S_{3/2}$ orbit of Er^{3+} and $3T_1$ level of the V 3d orbital, leading to oscillator strength increase in of the Er^{3+} ions.²³ We should stress that Tolstik et al.²⁴ measured lifetimes of 28 μs and 2.3 ms of the $^4I_{11/2}$ and $^4I_{13/2}$ levels of the Er^{3+} ion in YVO_4 hosts, respectively. Both lifetimes are significantly lower than in Y_2O_3 and other host matrices^{22,25} and could be responsible for the relative intensity reduction of the red emission band in samples hosted by YVO_4 , causing the stronger green emission.

The CIE (international commission on illumination) diagram provide the parameters x and y to demonstrate the color perception. This includes the hue and saturation on a two dimensional chromaticity diagram. We have given the color coordinates of $Y_{1.894}Yb_{0.1}Er_{0.006}O_3$, $Y_{0.947}Yb_{0.05}Er_{0.003}VO_4$ and $Y_{0.947}Yb_{0.05}Er_{0.003}PO_4$ in the CIE diagram shown in Fig 6 (a). The color perception reveals green (0.23, 0.74), yellowish (0.31, 0.67) blue-yellowish (0.30, 0.47) colors for the $Y_{0.947}Yb_{0.05}Er_{0.003}VO_4$, $Y_{1.894}Yb_{0.1}Er_{0.006}O_3$ and $Y_{0.947}Yb_{0.05}Er_{0.004}PO_4$ phosphors, respectively. It suggests that the color of the UC emission can also be tuned by modifications of the host lattices.

3.3 Temperature sensing

In the Er^{3+} ion, the $^2H_{11/2}$ and $^4S_{3/2}$ levels are thermally coupled to each other and the intensity ratio (R) of the $^2H_{11/2} \rightarrow ^4I_{15/2}$ and $^4S_{3/2} \rightarrow ^4I_{15/2}$ emission bands is expressed as a function of temperature for temperature measurements. Figure 6 (b) shows the UC emission temperature dependence of $Y_{0.945}Yb_{0.05}Er_{0.005}PO_4$ in the wavelength range 500–575 nm. While the peak positions do not reveal sensitivity to temperature alterations, R considerably changes. At temperatures below ~ 370 K the emission of $^2H_{11/2} \rightarrow ^4I_{15/2}$ band is less intense than the one of $^4S_{3/2} \rightarrow ^4I_{15/2}$ transition. For elevated temperatures beyond ~ 470 K, however, the situation is

opposite. The relative populations of the ${}^2\text{H}_{11/2}$ and ${}^4\text{S}_{3/2}$ levels follow the Boltzmann type distribution function, which leads to,

$$R = \frac{I_{523}}{I_{548}} = \frac{N({}^2\text{H}_{11/2})}{N({}^4\text{S}_{3/2})} = B \exp\left(\frac{-\Delta E}{kT}\right), \quad (1)$$

where, I_{523} and I_{548} are the integrated intensity of the ${}^2\text{H}_{11/2} \rightarrow {}^4\text{I}_{15/2}$ (515-540 nm) and ${}^4\text{S}_{3/2} \rightarrow {}^4\text{I}_{15/2}$ (540-565 nm) bands, N is the number of ions, and $B = \omega_{\text{H}} \cdot A_{\text{H}} \cdot g_{\text{H}} / \omega_{\text{S}} \cdot A_{\text{S}} \cdot g_{\text{S}}$, with ω , A , g being the transition frequency, spontaneous emission rate from ${}^2\text{H}_{11/2}$ and ${}^4\text{S}_{3/2}$ to the ground level ${}^4\text{I}_{15/2}$, and the level degeneracy, respectively - and k is the Boltzmann factor, T is the temperature, and ΔE is the energy gap between the ${}^2\text{H}_{11/2}$ and ${}^4\text{S}_{3/2}$ levels.

Figure 7(a) shows $R(T)$ for (i) $\text{Y}_{0.947}\text{Yb}_{0.05}\text{Er}_{0.003}\text{VO}_4$, (ii) $\text{Y}_{1.894}\text{Yb}_{0.1}\text{Er}_{0.006}\text{O}_3$, and (iii) $\text{Y}_{0.947}\text{Yb}_{0.05}\text{Er}_{0.003}\text{PO}_4$. As expected, caused by the above discussed differences of the recombination behaviors in Fig. 3, R varies for all the three samples. Additionally, the $R(T)$ trend can also be affected by change of non-radiative relaxation rates during the temperature increase, causing variations of the luminescence intensities and lifetimes of the single transitions.

The R fits displayed by the solid lines in Fig. 7 (a) results in $\Delta E/k$ fit parameters of (i) 598, (ii) 599, and (ii) 581 for $\text{Y}_{0.947}\text{Yb}_{0.05}\text{Er}_{0.003}\text{VO}_4$, $\text{Y}_{1.894}\text{Yb}_{0.1}\text{Er}_{0.006}\text{O}_3$, and $\text{Y}_{0.947}\text{Yb}_{0.05}\text{Er}_{0.003}\text{PO}_4$, respectively. The result demonstrates the proximity of the average energy gap between the levels ${}^2\text{H}_{11/2}$ and ${}^4\text{S}_{3/2}$ in all three investigated phosphors. The sensitivity (S) of the sensor is defined as,

$$S = \frac{dR}{dT} = R \left(\frac{\Delta E}{kT^2} \right). \quad (2)$$

where the symbols have the same meanings as in Eq. (1). Figures 7 (b)-(d) presents the calculated $S(T)$ trend. The maximum sensitivity in $\text{Y}_{0.947}\text{Yb}_{0.05}\text{Er}_{0.003}\text{VO}_4$, $\text{Y}_{1.894}\text{Yb}_{0.1}\text{Er}_{0.006}\text{O}_3$,

and $\text{Y}_{0.947}\text{Yb}_{0.05}\text{Er}_{0.003}\text{PO}_4$ phosphors is found to be 0.0105, 0.0077, 0.0035 K^{-1} at 499, 488, and 486 K, respectively.

It is important to mention that the temperature sensitivity in $\text{Y}_{0.947}\text{Yb}_{0.05}\text{Er}_{0.003}\text{PO}_4$ phosphor is significantly lower than in other two phosphors. This might be because of the higher phonon energy of the host lattice, which increases non-radiative relaxation from the $^2\text{H}_{11/2}$ to the $^4\text{S}_{3/2}$ level, resulting in the increase in the intensity of 548 nm emission with respect to the 523 nm emission (leading to smaller R). The value of 0.0105 maximum sensitivity observed in $\text{Y}_{0.947}\text{Yb}_{0.05}\text{Er}_{0.003}\text{VO}_4$ is probably the highest sensitivity reported for the luminescence intensity ratio based temperature sensors.¹⁻¹² The maximum sensitivity in all the three phosphors is observed $\sim 490\text{K}$, while, above this temperature, sensitivity starts to decrease. This might be because of the resonance of thermal phonon energy with the energy separation of the levels and/or the population saturation of the $^2\text{H}_{11/2}$ level at increasing temperatures.

4. Conclusion

Summarizing, x-ray data analysis reveals the cubic structure for $\text{Y}_{1.894}\text{Yb}_{0.1}\text{Er}_{0.006}\text{O}_3$ and the tetragonal structure for $\text{Y}_{0.947}\text{Yb}_{0.05}\text{Er}_{0.003}\text{VO}_4$ and $\text{Y}_{0.947}\text{Yb}_{0.05}\text{Er}_{0.003}\text{PO}_4$. The optical studies show that the phonon energy and crystal structure of the host lattices affect the UC emission intensity of the blue, green and red emission bands, as well as the Stark splitting of the levels. The R value in $\text{Y}_{0.947}\text{Yb}_{0.05}\text{Er}_{0.003}\text{PO}_4$ is significantly lower than in $\text{Y}_{1.894}\text{Yb}_{0.1}\text{Er}_{0.006}\text{O}_3$ and $\text{Y}_{0.947}\text{Yb}_{0.05}\text{Er}_{0.003}\text{VO}_4$ because of the higher phonon energy in $\text{Y}_{0.947}\text{Yb}_{0.05}\text{Er}_{0.003}\text{PO}_4$, enforcing faster relaxation from the $^2\text{H}_{11/2}$ to the $^4\text{S}_{3/2}$ level. The maximum temperature sensitivity in all the three phosphors takes place in the vicinity of 490 K, which is the highest (0.0105 K^{-1}) in $\text{Y}_{0.947}\text{Yb}_{0.05}\text{Er}_{0.003}\text{VO}_4$.

Acknowledgements

PKS acknowledges UGC, India for the award of JRF fellowship. AKS thankfully acknowledges the DGAPA-UNAM program of post-doctoral fellowship. The work was partly supported by the DGAPA-UNAM PAPIIT project TB100213-RR170213 (PI Dr. Bruno Ullrich). The authors also thankfully acknowledge DST, New Delhi for experimental facilities. The authors also acknowledge S. K. Singh for his support during the experiments and valuable discussions.

Supporting Information

UC emission spectra of $Y_{1.994}Er_{0.006}O_3$, $Y_{(1.9-2x)}Yb_{0.1}Er_{2x}O_3$, $Y_{(0.95-x)}Yb_{0.05}Er_xVO_4$ and $Y_{(0.95-x)}Yb_{0.05}Er_xPO_4$ ($x=0.003, 0.01$ and 0.02) phosphors and luminescence decay curves of $^4S_{3/2}$ level of Er^{3+} ion in $Y_{1.894}Yb_{0.1}Er_{0.006}O_3$, $Y_{0.947}Yb_{0.05}Er_{0.003}VO_4$ and $Y_{0.947}Yb_{0.05}Er_{0.003}PO_4$ phosphors are given in supporting information.

Authors' contributions

The manuscript was written through the contributions of all the authors. A.K.S. and P.K.S. have contributed equally to this work and therefore both are the first author of this manuscript. All the authors have given approval to the final version of the manuscript.

References

1. C. D. S. Brites, P. P. Lima, N. J. O. Silva, A. Milla'n, V. S. Amaral, F. Palacio and L. D. Carlos, *New J. Chem.*, 2011, **35**, 1177–1183.
2. F. Vetrone, R. Naccache, A. Zamarro'n, A. J. de la Fuente, F. Sanz-Rodr'iguez, L. Martinez Maestro, E. M. Rodriguez, D. Jaque, J. G. Sole' and J. A. Capobianco, *ACS Nano*, 2010, **4**, 3254-3258.
3. L. H. Fischer, G. S. Harms and O. S. Wolfbeis, *Angew. Chem. Int. Ed.* 2011,**50**, 4546-4551.
4. H. Peng, M.I.J. Stich, J. Yu, L. Sun, L.H. Fischer and O.S. Wolfbeis, *Adv. Mater.*, 2010,**22**, 716-719.

5. A.K. Singh, S.K. Singh, B.K. Gupta, R. Prakash and S.B. Rai, *Dalton Trans.*, 2013, **42**, 1065-1072.
6. B. Dong, B. Cao, Y. He, Z. Liu, Z. Li and Z. Feng, *Adv. Mater.* 2012, **24**, 1987-1993.
7. R. Dey and V. K. Rai, *Dalton Trans.*, 2014, **43**, 111-118.
8. S. K. Singh, K. Kumar, S.B. Rai, *Sensors and Actuat. A* 2009, **149**, 16.
9. X. Wang, J. Zheng, Y. Xuan and X. Yan, *Optics Express*, 2013, **21**, 21596-21606.
10. A. Pandey and V. K. Rai, *Dalton Trans.*, 2013, **42**, 11005-11011.
11. J. B. Yu, L. N. Sun, H. S. Peng and M. I. J. Stich, *J. Mater. Chem.*, 2010, **20**, 6975–6981.
12. B. Zelelow, G. E. Khalil, G. Phelan, B. Carlson, M. Gouterman, J. B. Callis and L. R. Dalton, *Sens. Actuators B*, 2003, **96**, 304–314.
13. F. Wang and X. Liu, *Chem. Soc. Rev.*, 2009, **38**, 976–989.
14. A.K. Singh, S.K. Singh, P. Kumar, B.K. Gupta, R. Prakash and S.B. Rai, *Sci. Adv. Mater.*, 2014, **6**, 405-412.
15. F. Auzel, *Chem. Rev.*, 2004, **104**, 139-173.
16. A. K. Singh, S. K. Singh and S. B. Rai, *RSC Adv.*, 2014, **4**, 27039-27061.
17. J. Rodriguez-Carvajal *FULLPROF a Rietveld and pattern matching analysis program* Laboratoire Leon Brillouin (CEA-CRNS): France, 2007.
18. K. Mishra, S.K. Singh, A.K. Singh and S.B. Rai, *Mater. Res. Bull.*, 2013, **48**, 4307–4313.
19. A.K. Parchur, A.I. Prasad, S.B. Rai, R. Tewari, R.K. Sahu, G.S. Okram, R.A. Singh and R.S. Ningthoujam, *AIP Adv.*, 2012, **2**, 032119.
20. B. F. Aull and H. P. Jenssen, *Phys. Rev. B*, 1986, **34**, 6640-6646.
21. L. Sorace, C. Benelli and D. Gatteschi, *Chem. Soc. Rev.*, 2011, **40**, 3092-3104.
22. H. Lu, W. P. Gillin and I. Hernandez, *Phys. Chem. Chem. Phys.*, 2014, **16**, 20957-20963.

23. W. Xu, B. Chen, W. Yu, Y. Zhu, T. Liu, S. Xu, X. Min, X. Bai and H. Song, *Dalton Trans.*, 2012, **41**, 13525-13532.
24. N. A. Tolstik, A.E. Troshin, S. V. Kurilchik, V.E. kisel, N.V. Kuleshov, V.N. Matrosov, T.A. matrosova and M.I. Kupchenko, *Appl. Phys. B*, 2007, **86**, 275–278.
25. A. Jaffrès, P. Loiseau, G. Aka, B. Viana, C. Larat and E. Lallier, *Laser Phys.*, 2014, **24**, 125801.

Table: 1 Refine structural parameters for $Y_{1.894}Yb_{0.1}Er_{0.006}O_3$ (space group = $Ia-3$), $Y_{0.947}Yb_{0.05}Er_{0.003}VO_4$ (space group = $I41/amd$) and $Y_{0.947}Yb_{0.05}Er_{0.003}PO_4$ (space group = $I41/amd$) phosphors.

Sample	Atoms	Positional Coordinates			Occupancy	Thermal Parameters B (\AA^2)
		X	Y	Z		
$Y_{1.894}Yb_{0.1}Er_{0.006}O_3$	Y/Yb/Er	0.25(0)	0.25(0)	0.25(0)	1.0	0.63(7)
	Y/Yb/Er	0.968(2)	0.00(0)	0.25(0)	1.0	0.45(5)
	O	0.392(1)	0.156(2)	0.376(2)	3.0	0.41(8)

$$a=b=c=10.5935(2) \text{ \AA}, R_p=12.0, R_{wp}=16.9, R_{exp}=11.74, \chi^2=2.06$$

Y-O=2.4441 \AA (48), Y-Y=3.5138 \AA (48), Y-Y=3.9923 \AA (24), Y-Y=3.5302 \AA (48), Y-O=2.2717 \AA (48), Y-O=2.3904 \AA (48), O-Y=2.2437 \AA (24), Y-Y=4.0064 \AA (24)

$Y_{0.947}Yb_{0.05}Er_{0.003}VO_4$	Y/Yb/Er	0.00(0)	0.75(0)	0.125(0)	1.0	0.70(4)
	V	0.00(0)	0.25(0)	0.375(0)	1.0	0.08(1)
	O	0.00(0)	0.435(1)	0.203(1)	4.0	0.13(2)

$$a = b = 7.1112 (2) \text{ \AA}, c = 6.2860(2) \text{ \AA}, R_B = 8.9, R_{wp} = 11.3, R_{exp} = 4.98, \chi^2 = 5.14$$

Y-Y=3.8842 \AA (5), Y-V=3.1405 \AA (6), Y-O=2.2882 \AA (14), Y-O=2.4352 \AA (12), V-O=1.7088 \AA (16)

$Y_{0.947}Yb_{0.05}Er_{0.003}PO_4$	Y/Yb/Er	0.00(0)	0.75(0)	0.125(0)	1.0	0.60(4)
	P	0.00(0)	0.25(0)	0.375(0)	1.0	0.09(1)
	O	0.00(0)	0.426(1)	0.219(1)	4.0	0.23(2)

$$a = b = 6.818(2) \text{ \AA}, c = 6.0187(2) \text{ \AA}, R_B = 9.16, R_{wp} = 12.7, R_{exp} = 4.69, \chi^2 = 7.3$$

Y-Y=3.7555 \AA (5), Y-P=3.0092 \AA (6), Y-O=2.30122 \AA (14), Y-O=2.3964 \AA (12), P-O=1.15325 \AA (16)

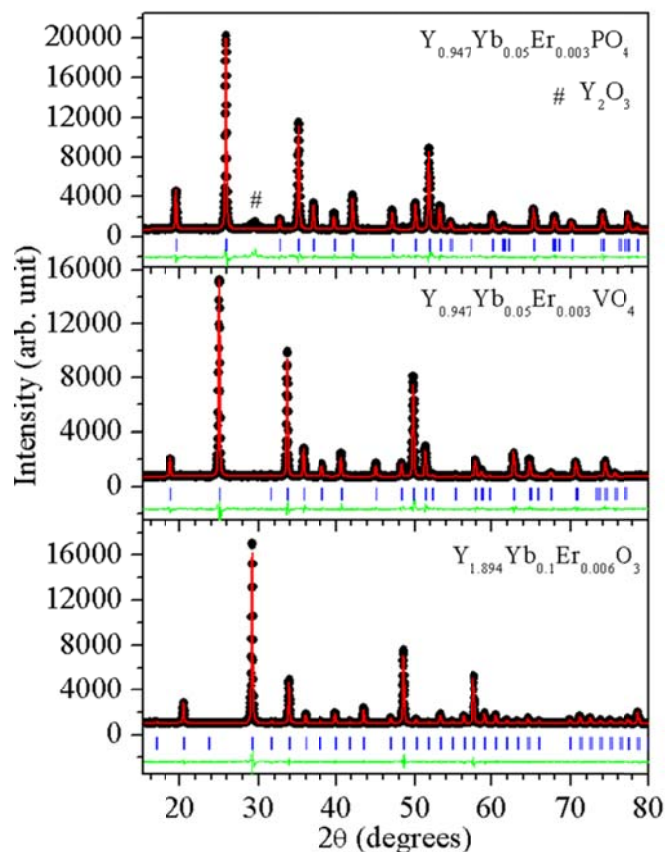


Figure 1: X-ray diffraction patterns of the $\text{Y}_{1.894}\text{Yb}_{0.1}\text{Er}_{0.006}\text{O}_3$, $\text{Y}_{0.947}\text{Yb}_{0.05}\text{Er}_{0.003}\text{VO}_4$ and $\text{Y}_{0.947}\text{Yb}_{0.05}\text{Er}_{0.003}\text{PO}_4$ phosphors: The experimental results are represented by dots, and the solid lines show the calculation and difference (bottom) profiles after Rietveld refinement. Vertical tick marks above the difference plot show the positions of the Bragg peaks.

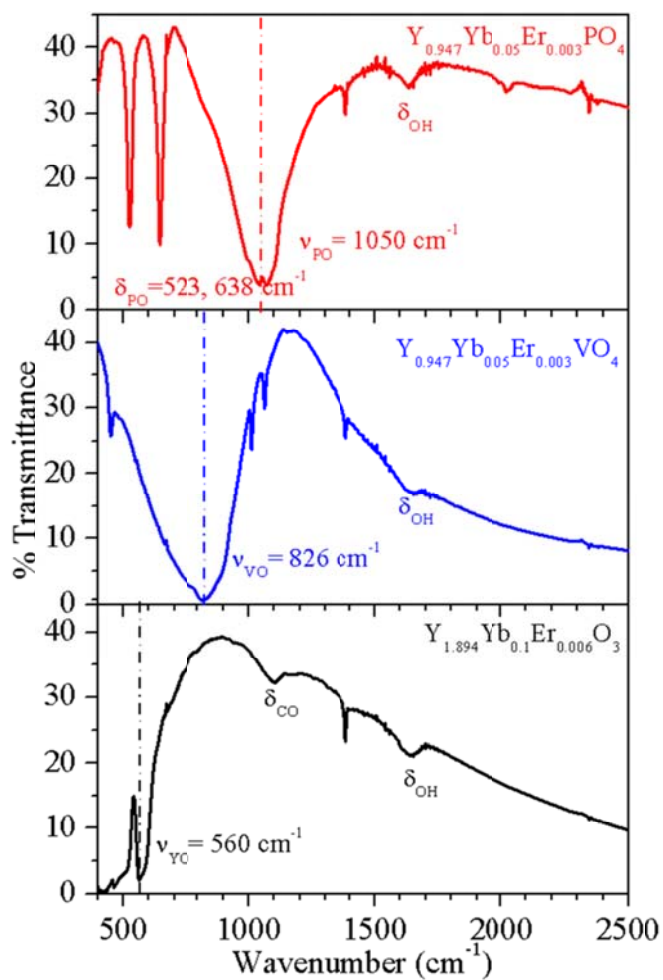


Figure 2: FTIR spectrum of $\text{Y}_{1.894}\text{Yb}_{0.1}\text{Er}_{0.006}\text{O}_3$, $\text{Y}_{0.947}\text{Yb}_{0.05}\text{Er}_{0.003}\text{VO}_4$ and $\text{Y}_{0.947}\text{Yb}_{0.05}\text{Er}_{0.003}\text{PO}_4$ phosphors.

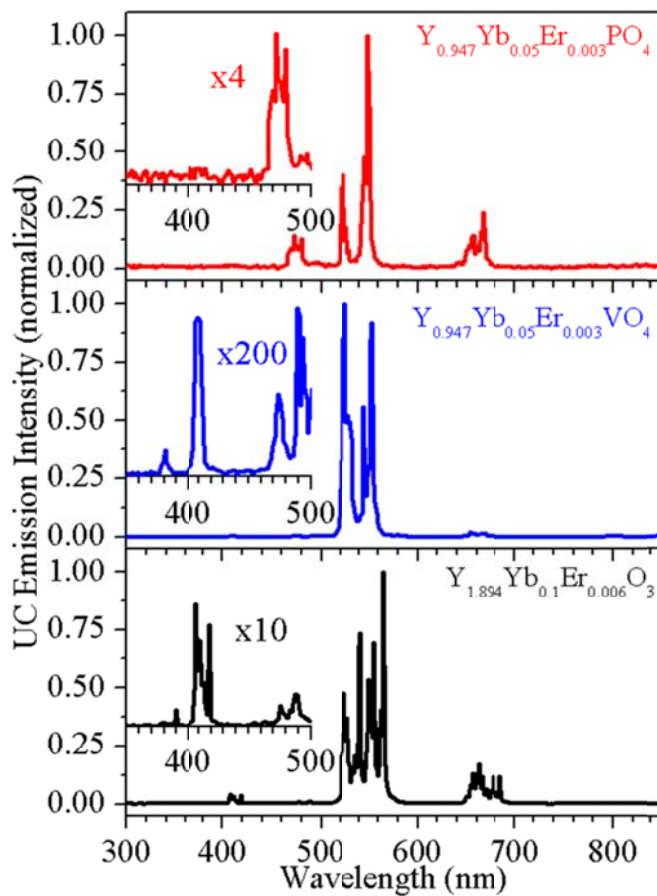


Figure 3: Room temperature UC emission spectrum of $Y_{1.894}Yb_{0.1}Er_{0.006}O_3$, $Y_{0.947}Yb_{0.05}Er_{0.003}VO_4$ and $Y_{0.947}Yb_{0.05}Er_{0.003}PO_4$ phosphors.

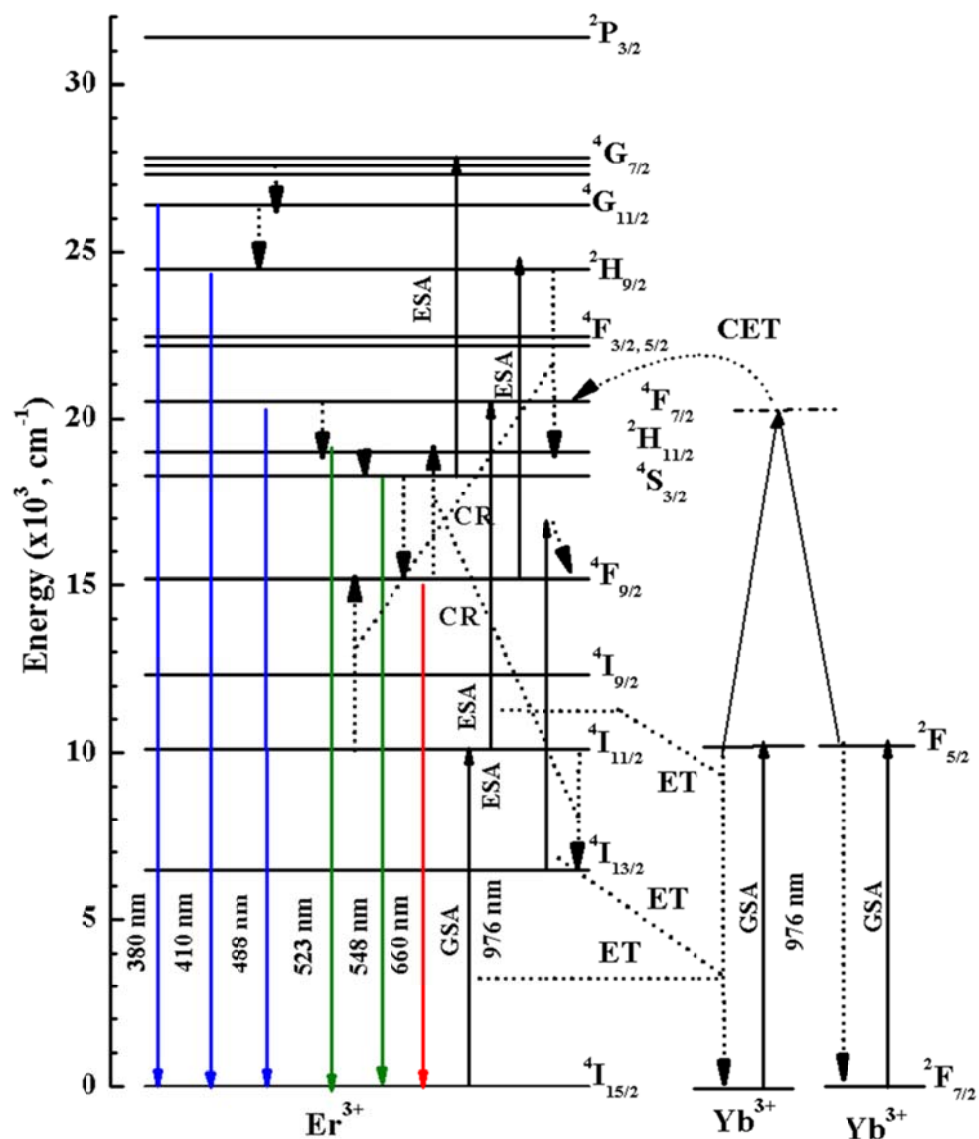


Figure 4: Schematic energy level diagram of Er^{3+} - Yb^{3+} showing mechanism involved in UC emissions.

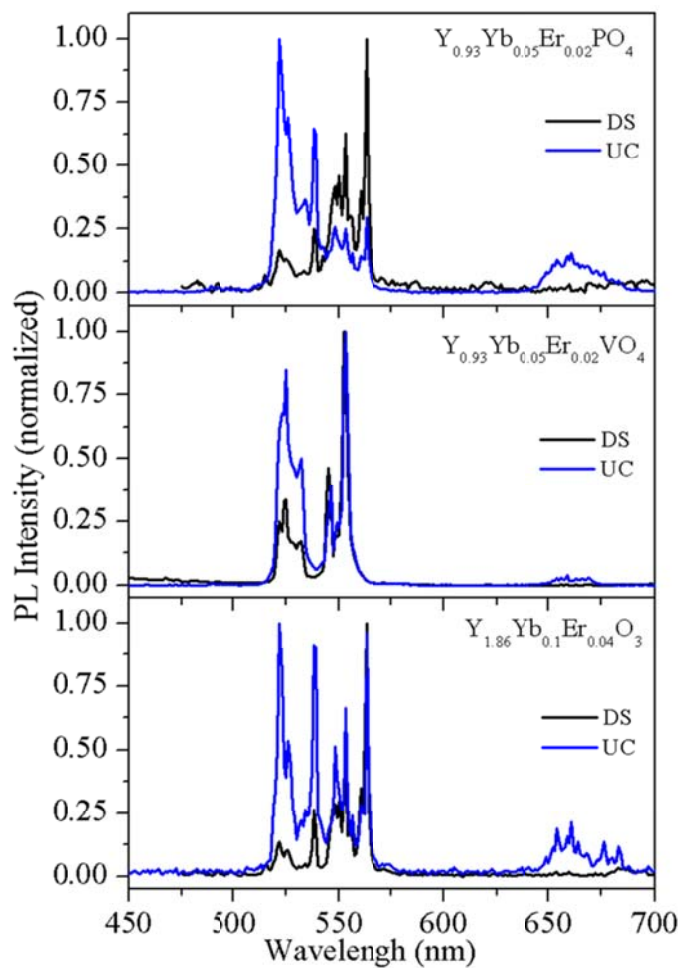


Figure 5: Room temperature DS and UC emission spectra of the $Y_{1.86}Yb_{0.1}Er_{0.04}O_3$, $Y_{0.93}Yb_{0.05}Er_{0.02}VO_4$, and $Y_{0.93}Yb_{0.05}Er_{0.02}PO_4$ phosphors.

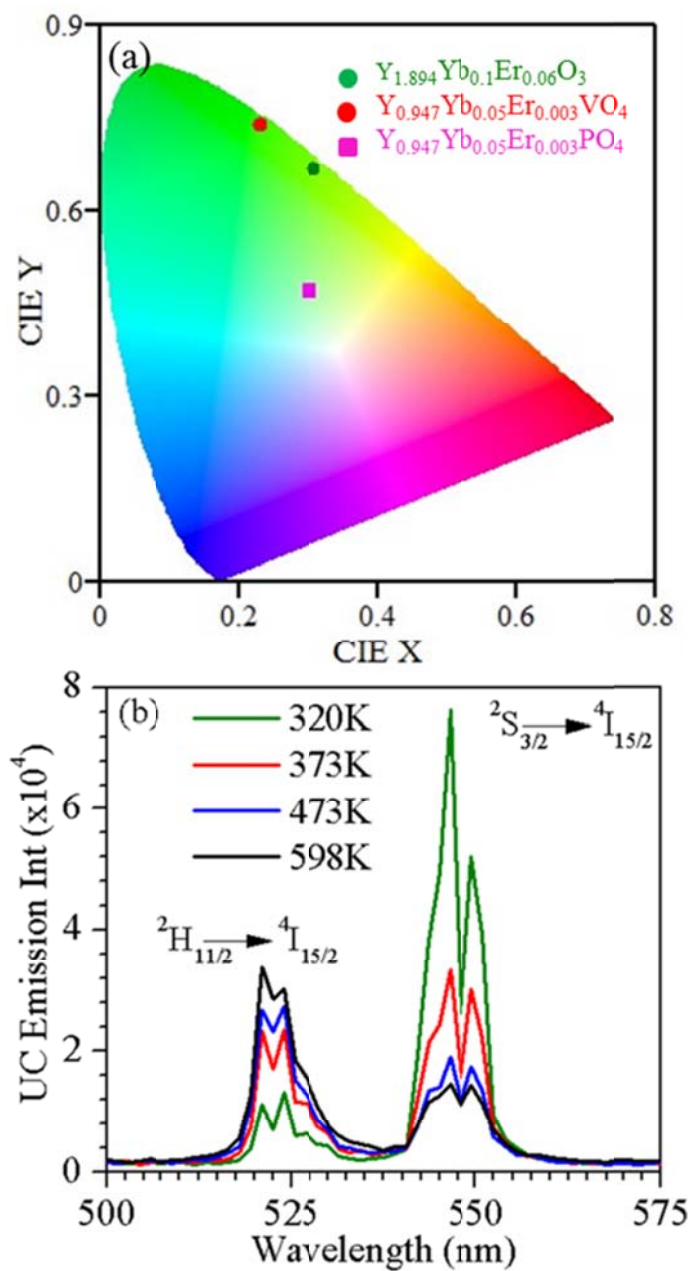


Figure 6: (a) The CIE chromaticity diagram for the UC emission in $Y_{1.894}Yb_{0.1}Er_{0.006}O_3$, $Y_{0.947}Yb_{0.05}Er_{0.003}VO_4$ and $Y_{0.947}Yb_{0.05}Er_{0.003}PO_4$. (b) The UC emission of $Y_{0.947}Yb_{0.05}Er_{0.003}PO_4$ measured at different temperatures.

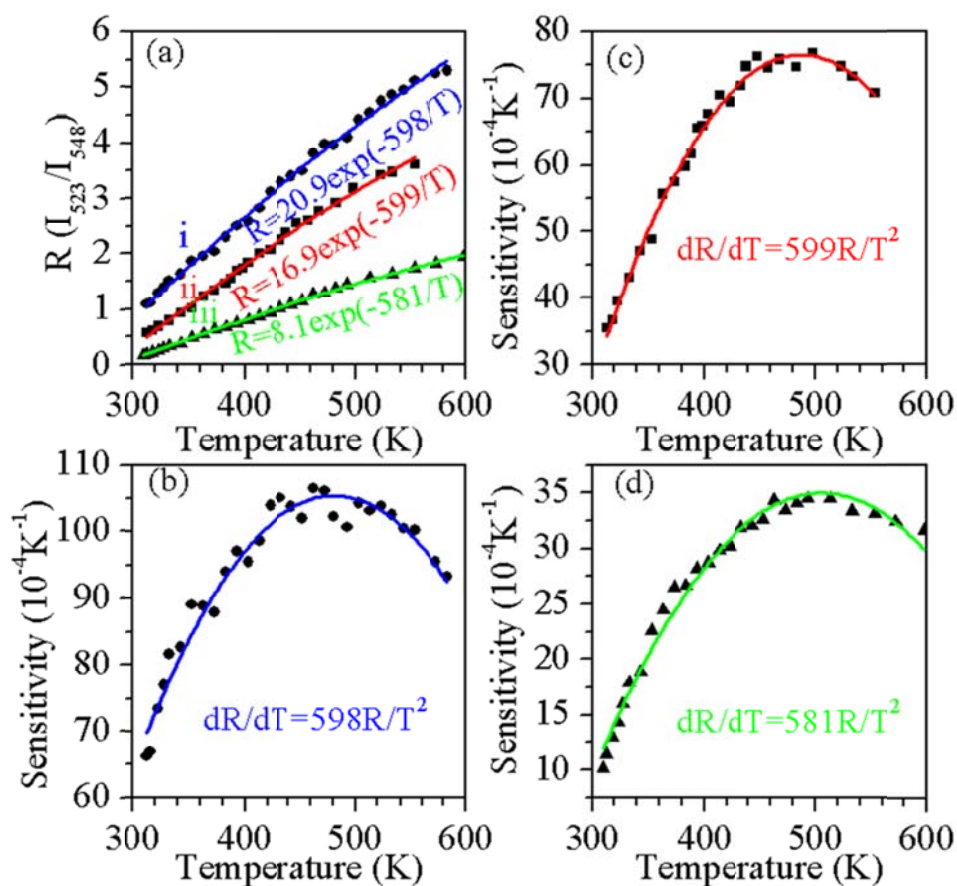


Figure 7: Temperature sensing performance of the samples: (a) R numbers of the 523 and 548 nm emission bands in (i) $\text{Y}_{0.947}\text{Yb}_{0.05}\text{Er}_{0.003}\text{VO}_4$, (ii) $\text{Y}_{1.894}\text{Yb}_{0.1}\text{Er}_{0.006}\text{O}_3$ and (iii) $\text{Y}_{0.947}\text{Yb}_{0.05}\text{Er}_{0.003}\text{PO}_4$, as a function of temperature. Temperature sensitivity in (b) $\text{Y}_{0.947}\text{Yb}_{0.05}\text{Er}_{0.003}\text{VO}_4$, (c) $\text{Y}_{1.894}\text{Yb}_{0.1}\text{Er}_{0.006}\text{O}_3$, and (d) $\text{Y}_{0.947}\text{Yb}_{0.05}\text{Er}_{0.003}\text{PO}_4$ vs. temperature.

Graphical Abstract

Impact of phonon frequency and crystal structure of the host lattice on upconversion emission.

